Check for
updates

A photocatalytic comparison study between tin complex and carboxylic acid derivatives of porphyrin/TiO$_2$ composites

Rangaraju Satish Kumar[1] · Hyorim Kim[1] · Naveen Mergu[1] · Young-A Son[1]

Abstract

We synthesized a novel dihydroxotin(IV) porphyrin complex with full structural confirmation. The tin complex further converted to TiO$_2$ composite (**PR-2–TiO$_2$**) and photodegradation of methylene blue property compared with carboxylic-anchored porphyrin photocatalyst (**PR-3–TiO$_2$**), basic porphyrin photocatalyst (**PR-1–TiO$_2$**) and bare **TiO$_2$**. **PR-1–TiO$_2$** showed slight photocatalytic activity, which was better than that of bare TiO$_2$. The photocatalytic performances of tin-porphyrin (**PR-2–TiO$_2$**) and carboxylic anchor porphyrin (**PR-3–TiO$_2$**) were comparable, and tin-porphyrin catalyst showed similar stability in their reusability test result in comparison with carboxylic-anchored porphyrin catalyst. Finally, we showed a plausible structure for the tin porphyrin complex between the axial –OH ligand and TiO$_2$ and a suitable mechanism with theoretical comparison for the photocatalytic process.
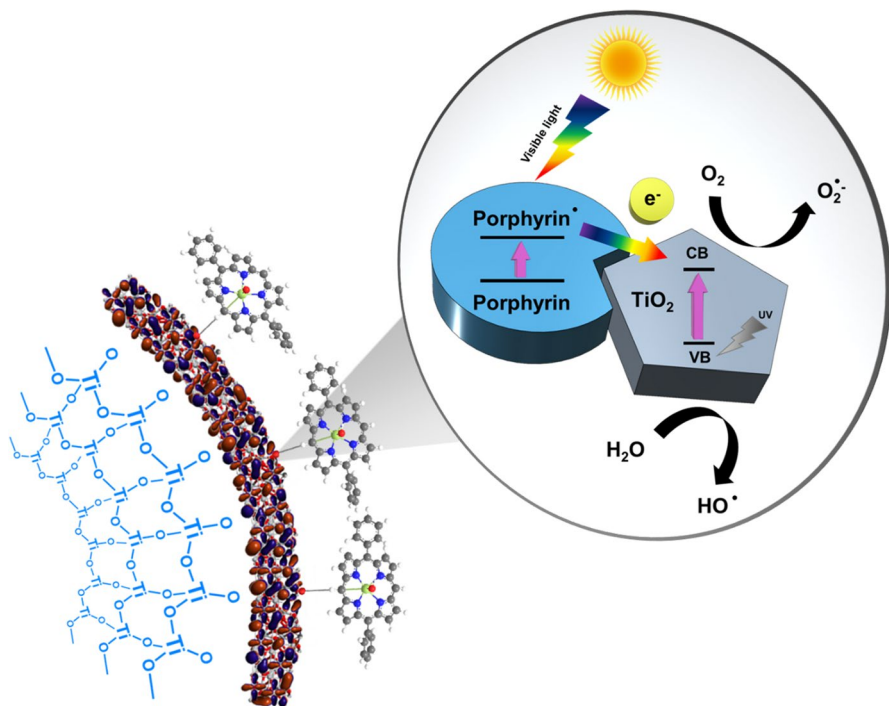
Rangaraju Satish Kumar and Hyorim Kim have contributed equally to this work.

✉ Young-A Son
   yason@cnu.ac.kr

1   Department of Advanced Organic Materials Engineering, Chungnam National University, 220 Gung-dong, Yuseong-gu, Daejeon 305-764, South Korea

Graphic abstract

Introduction

Titanium dioxide (TiO_2) plays a key role in chemical industries and environmental remediation through the photodegradation of organic pollutants [1–3]. Due to its band gap energy of 3.2 eV, anatase TiO_2 absorbs light at $\lambda < 387$ nm (UV region) to transfer the electrons from the valence band to the conduction band. In the solar spectrum, visible light is more abundant. To use the complete solar spectrum, various methods have been previously attempted, such as doping, sensitizing, surface modification and semiconductor coupling [4–7]. However, combining organic sensitizers with TiO_2 has been the best option for producing highly efficient photocatalysts. Porphyrin–TiO_2 photocatalysts have become a very attractive option in recent years because porphyrins are very good dyes with large π-electron conjugation and easy to synthesize in various substituted forms that have different photophysical properties and they have high extinction coefficient values in the visible region, which extends the light absorption capacity and shifts the band gap of TiO_2 to smaller values [8]. The previous literature has confirmed that the porphyrin–TiO_2

system has better visible light-driven photocatalytic activity in comparison with that of bare TiO_2 [9–11]. However, until now, mainly carboxylic acid-anchored porphyrin–TiO_2 systems have been well studied for photocatalysis [12].

Dihydroxotin(IV) porphyrins are hexa coordinated with hydroxy *trans*-diaxial ligands and are stable in acidic conditions. Tin porphyrins were first described by Carroll et al. [13], after which many research groups began work on tin porphyrin complexes [14, 15]. The excited state of tin porphyrin has a high affinity for electrons, which can initiate photooxidative processes. This is exactly the opposite behavior of zinc(II) porphyrin complexes, and these photooxidative abilities make dihydroxotin(IV) porphyrin an attractive environmental photocatalyst [16–18]. Inspired by a previous report on dihydroxotin(IV) porphyrin photocatalysts [19], our previous experience on porphyrin–TiO_2 studies [20–22] and porphyrin synthesis [23, 24], here we synthesized a new dihydroxo Sn(IV) porphyrin complex (**PR-2**). This PR-2 was combined with TiO_2 anatase, and the resulting **PR-2–TiO$_2$** photocatalytical results were compared with **PR-1–TiO$_2$**, **PR-3–TiO$_2$** and bare TiO_2 anatase (Fig. 1). Here, our strategy is a comparison study of the our previously reported carboxylic-anchored porphyrin photocatalyst, PR-3–TiO_2 [20], and our new axially coordinated hydroxyl-anchored photocatalyst for the degradation of methyl blue in water medium under visible light irradiation (663 nm). Simply, we discussed the influence of axial ligation on the photocatalytic effect.

Experimental section

Chemicals and equipment

All reagents and solvents were obtained from commercial sources and were spectroscopic or analytical grade. An AVANCE III 600 spectrometer (Akishima, Japan)
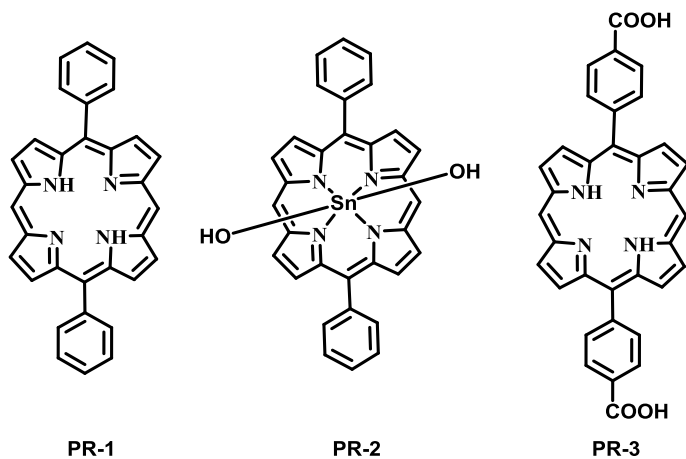

Fig. 1 Molecular structures of the **PR-1**, **PR-2** and **PR-3** dyes

was used for ^{1}H NMR and ^{13}C NMR spectral analysis at 600 MHz (^{1}H NMR) and 150 MHz (^{13}C NMR) by using Alice 4.0 software and CDCl$_3$ and DMSO-d_6 as solvents. Tetra methyl silane was used as an internal standard for the chemical shifts (parts per million). HRMS and MALDI-TOF analyses were conducted with a 1290 infinity II/Triple TOF 5600 plus mass spectrometer and a Bruker AutoFlex III mass spectrometer, respectively. The FTIR spectra were recorded with an ALPHA-P spectrometer. UV–visible absorption spectra were obtained with an Agilent 8453 spectrophotometer, and a Shimadzu SolidSpec-3700 was used to obtain solid-state diffuse reflectance UV–Vis spectra. For SEM analysis, a LYRA3 XMU instrument was used. An X-ray diffractometer (PHILIPS, X'Pert-MPD System, Max P/N: 3 kW/40 kV, 45 Ma, Netherlands) with a Cu, X-ray tube was used for the XRD studies. Transient fluorescence decay and excited state lifetime measurements were performed on Fluorolog3 with TCSPC (Horiba Scientifics) using PTI nanosecond pulsed LED (340 nm) as an excitation light source.

Synthesis

Synthesis of 5,15-diphenylporphyrin (PR-1)

Dipyrromethane (6.7 g, 20 mmol) and benzaldehyde (2.1 g, 20 mmol) were dissolved in 1000 mL of dichloromethane, and trifluoroacetic acid (1.14 g, 10 mmol) was added to the resulting mixture and then stirred for 4 h at room temperature. Then, 2,3-dichloro-5,6-dicyanobenzoquinone (6.8 g, 30 mmol) was added and stirred for another hour, and the reaction mixture was finally quenched with triethylamine (20 mL). The solvent was removed under vacuum distillation. The crude mixture was further purified by using silica gel column chromatography with hexane and DCM (1:1) to give compound **PR-1** as a purple solid (yield: 4.25 g, 46%). ^{1}H NMR (600 MHz, CDCl$_3$): δ 10.21 (s, 2H), 9.29 (d, $J = 4.5$ Hz, 4H), 8.99 (d, $J = 4.5$ Hz, 4H), 8.17–8.21(m, 4H), 7.70–7.75 (m, 6H), -3.19 (s, 2H) ppm; ^{13}C NMR (150 MHz, CDCl$_3$): δ 146.1, 144.1, 140.3, 133.8, 130.5, 130.0, 126.6, 125.9, 118.0, 104.2 ppm. IR (KBr tablet) ν_{max}/cm^{-1}: 3301, 3010, 2991, 1640, 1522, 1421, 1322, 1301, 1251, 899, 801, 780. HRMS (ESI–MS) m/z calcd for C$_{32}$H$_{23}$N$_4$ [M + H]$^+$: 463.1917, found 463.1910.

Dihydroxo(5,15-diphenylporphyrinato)tin(IV) (PR-2)

PR-1 (462 mg, 1 mmol) was dissolved in pyridine (120 mL), and tin (II) chloride dihydrate (451 mg, 2 mmol) was added slowly, and the reaction mixture was heated at reflux for 6 h. Then, the reaction mixture was concentrated and washed with excess water and ether, and the obtained crude product was dissolved in a RB flask with THF/water (8:2, 50 mL), and potassium carbonate (2.1 g, 15 mmol) was added. Afterward, stirring was continued for up to 4 h at reflux. To the reaction mixture, DCM (100 mL) was added, and the solution was washed with water (2 × 50 mL), and the product was finally recrystallized in hexane/chloroform (1:1) to obtain PR-2 as a purple solid (yield: 86%), ^{1}H NMR (600 MHz, CDCl$_3$): δ 10.81 (s, 2H), 9.75 (d,

$J = 4.3$ Hz, 4H), 9.32 (d, $J = 4.3$ Hz, 4H), 8.34–8.39(m, 4H), 7.85–7.94 (m, 6H) ppm; ^{13}C NMR (150 MHz, CDCl$_3$): δ 146.6, 145.7, 140.9, 135.3, 133.3, 132.3, 128.2, 127.1, 120.4, 105.7. IR (KBr tablet) ν_{max}/cm^{-1}: 3011, 2899, 1670, 1577, 1455, 1422, 1366, 1310, 1211, 865, 791. C$_{32}$H$_{22}$N$_4$O$_2$Sn; Calculated, %: C 62.67; H 3.62; N 9.14, Found, %: C 62.64; H 3.64; N 9.11. MS (MALDI-TOF): 614.512 [M]$^+$.

Synthesis of porphyrin-grafted TiO$_2$

TiO$_2$ nanoparticles were prepared according to our previous report [20]. All the photocatalysts were prepared according to the following procedure. A TiO$_2$ anatase (2.0 g), dye (100 mg) and DMF (250 mL) solution were heated at reflux for 15 h. The reaction was covered with aluminum foil to avoid light exposure. The resultant reaction mixture was filtered, and the solid was washed with excess distilled water. Finally, the collected solid was dried under vacuum for 24 h at 50 °C.

Methods for photocatalytic experiments

The photocatalytic experiments were conducted by using a Model XPA-VII photocatalytic instrument [20]. Methylene blue (MB) (8 mg) and photocatalyst (50 mg) were dispersed in water (500 mL), and before light irradiation, the solution was continuously stirred under dark condition for 30 min to get adsorption–desorption equilibrium. Afterward, for simulation of visible light, the samples were irradiated with a 400 W halogen lamp with maintaining room temperature inside the reactor. The halogen lamp was placed in a quartz socket tube with one end closed. The average light intensity on the surface of the sample was approximately 615 mW cm^{-2}. Every 30 min, up to 180 min, 5 mL of the sample was withdrawn from the suspension. The nanoparticles from the withdrawn suspension were precipitated via centrifugation at 5000 rpm for 20 min. By using the filtered solution, UV–visible absorption spectra were recorded at 663 nm.

Results and discussion

Synthesis of dyes

To synthesize PR-1, we reacted dipyrromethane and benzaldehyde in the presence of TFA (trifluoroacetic acid) and DDQ (2,3-dichloro-5,6-dicyanobenzoquinone), and we obtained **PR-1** as a purple solid in good yield. This PR-1 was further reacted with tin(II) chloride dihydrate in pyridine to obtain a crude axially coordinated dichloro derivative, and without any purification, this product was reacted with potassium carbonate in a water and THF mixture to obtain our targeted hydrolysis product PR-2 (Scheme 1). For PR-3, we used our previously reported procedure [20]. All the synthesized dyes were fully confirmed by ^{1}H NMR, ^{13}C NMR, FTIR, elemental analysis and MALDI-TOF mass analytical methods.
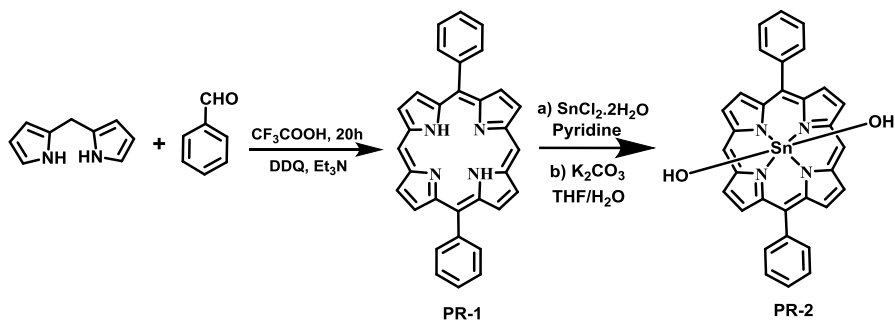
Scheme 1 Synthesis of axial dihydroxy tin porphyrin **(PR-2)**

Scanning electron microscopy (SEM) analysis and XRD patterns of the photocatalysts

All of the photocatalyst surface morphologies were analyzed by SEM, and representative images are depicted in Fig. 2. In comparison with that of bare TiO_2, the remaining photocatalysts (PR-1–TiO_2, PR-2–TiO_2 and PR-3–TiO_2) showed different surface morphologies because of the dispersion of the porphyrin moieties
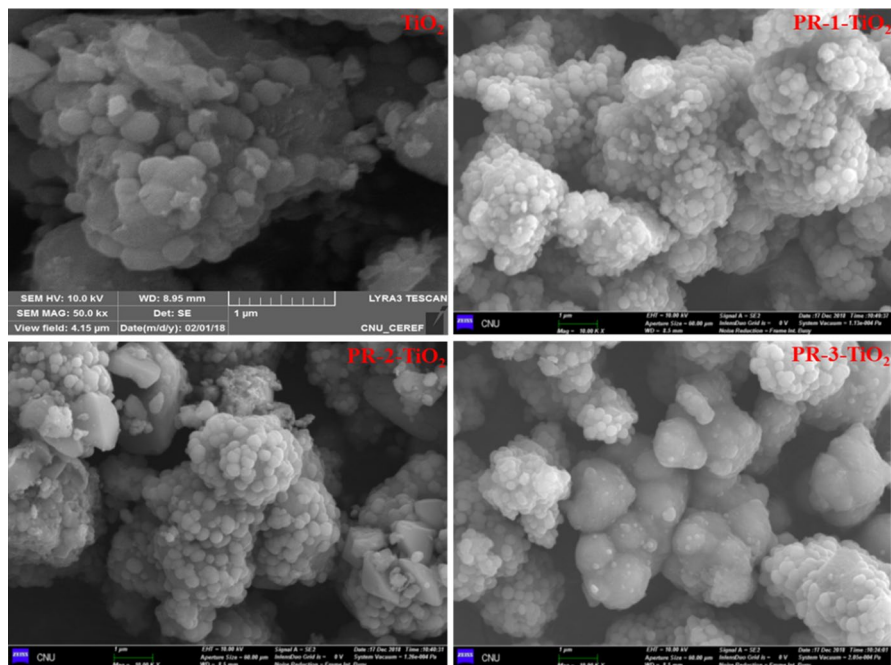
Fig. 2 SEM images (1 µm) of bare TiO_2, PR-1–TiO_2, PR-2–TiO_2 and PR-3–TiO_2 photocatalysts

[25]. The SEM images indicate that the porphyrins have nicely penetrated the TiO_2 surface for the PR-1–TiO_2, PR-2–TiO_2 and PR-3–TiO_2 photocatalysts.

For bare TiO_2, the peaks observed at 2θ values of 24.9°, 37.5°, 48.3°, 54.5°, 63.1°, 69.5° and 75.5° can be indexed to the (101) (004), (200), (211), (002), (301) and (215) faces of anatase TiO_2, respectively [26]. As shown in Fig. 3, PR-1–TiO_2, PR-2–TiO_2 and PR-3–TiO_2 displayed similar patterns as that of bare anatase TiO_2, indicating that the porphyrin photocatalysts formed without any disturbance of the TiO_2 nanostructure.

Diffused reflectance spectra of photocatalysts

Figure 4 shows the diffuse reflectance spectra of bare TiO_2, PR-1–TiO_2, PR-2–TiO_2 and PR-3–TiO_2 in the range of 250–800 nm. Bare TiO_2 shows a UV–Vis absorption region below 400 nm because TiO_2 absorbs only UV light, and in our experiment, we also observed the same behavior for bare TiO_2. In the case of PR-1–TiO_2, PR-2–TiO_2 and PR-3–TiO_2, absorption peaks in the region of 400 nm to 700 nm were observed, which are the characteristic peaks of the porphyrins [27]. These results indicate that the porphyrins have been loaded onto the surface of TiO_2 without any loss in their basic structure.
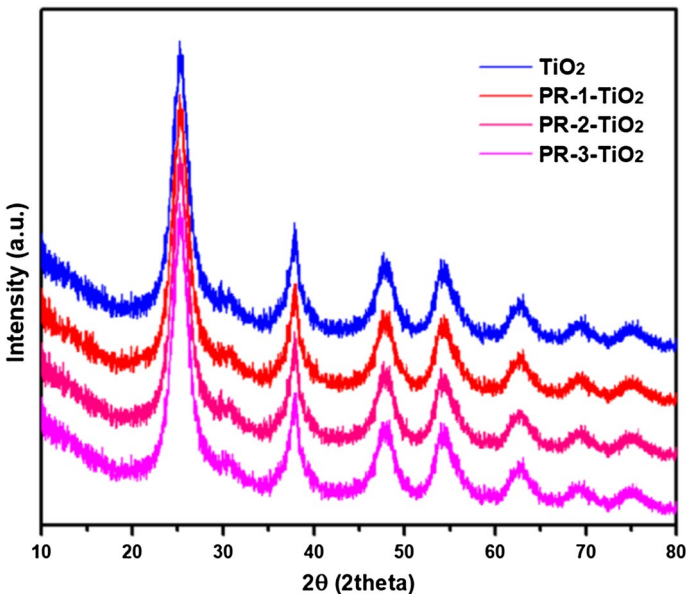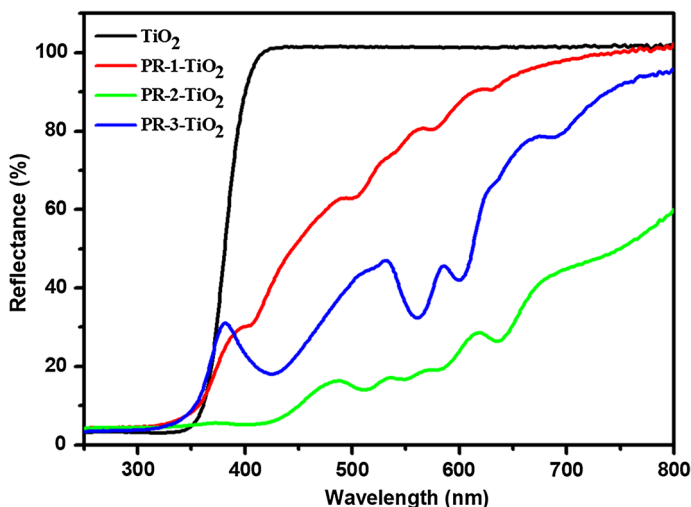

Fig. 3 XRD patterns of bare TiO_2, PR-1–TiO_2, PR-2–TiO_2 and PR-3–TiO_2 photocatalysts

X-ray photoelectron spectroscopy (XPS) analysis of photocatalysts

To confirm the elemental composition and binding energies, we performed XPS analysis of bare TiO$_2$, PR-1–TiO$_2$, PR-2–TiO$_2$ and PR-3–TiO$_2$. For bare TiO$_2$, we observed a 1:2 ratio for Ti and O. For PR-1–TiO$_2$ and PR-3–TiO$_2$, we found N, C, Ti and O atoms. PR-2–TiO$_2$ showed a peak corresponding to Sn atoms at a binding energy of 486.43 eV, which belongs to the $3d_{5/2}$ peak of Sn(II and IV), and this binding energy perfectly matches that of a previous reports [28, 29]. Although this binding energy represents both Sn(II) and Sn(IV), we assigned it to Sn(IV) because Sn(II) is highly air sensitive and very unstable at room temperature (Fig. 5).

To further understand the binding energy changes of Ti 2p, we compared the XPS results of bare TiO$_2$ with those of PR-1–TiO$_2$, PR-2–TiO$_2$ and PR-3–TiO$_2$. The Ti 2p band of bare TiO$_2$ is observed at 457.2 eV. For PR-1–TiO$_2$, PR-2–TiO$_2$ and PR-3–TiO$_2$, the Ti 2p peak is seen at 457.6 eV, 457.9 eV and 457.8 eV. We observed a slight increase in the binding energies of the porphyrin photocatalysts in comparison with that of bare TiO$_2$ because Ti acts as an electron accepting element and withdraws electrons from the porphyrin (Fig. 6) [30, 31].

Photodegradation results

Generally, many of the organic compounds were used in various industries contaminate rivers, ponds and underground water sources. For this reason, to determine the photocatalytic properties of our photocatalysts, we selected methylene blue in water medium as a sample organic pollutant for photocatalysis under visible light conditions. Figure 7a shows the degradation results, and Fig. 7b displays the UV–Vis spectra for photodegradation for PR-2–TiO$_2$. In the case of bare anatase TiO$_2$, we observed insignificant decrease in the absorption maxima at the

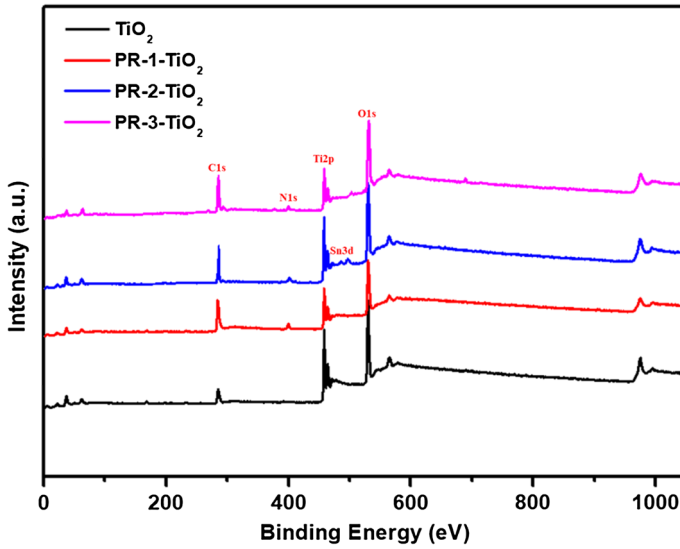**Fig. 5** XPS survey spectra of the bare TiO_2, PR-1–TiO_2, PR-2–TiO_2 and PR-3–TiO_2 photocatalysts
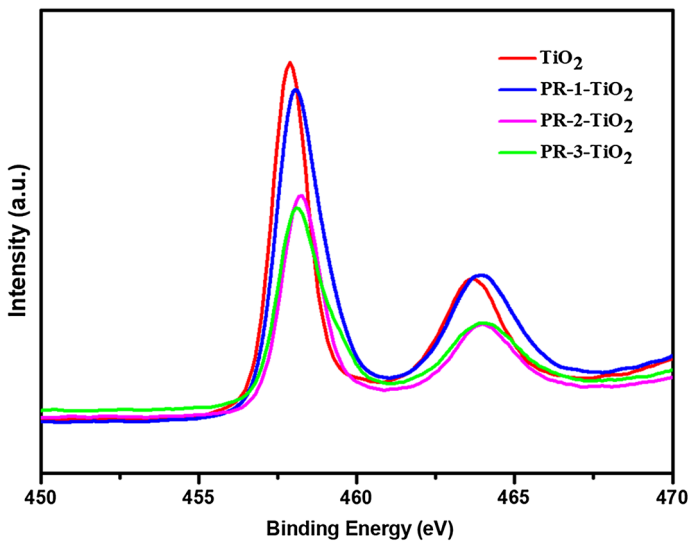
Fig. 6 The Ti 2*p* binding energy spectra for bare TiO_2, PR-1–TiO_2, PR-2–TiO_2 and PR-3–TiO_2 as measured by XPS

663 nm peak of MB, for basic porphyrin (PR-1–TiO_2), we observed an almost 30% reduction, whereas the porphyrin tin photocatalyst (PR-2–TiO_2) and carboxylic-anchored porphyrin (PR-3–TiO_2) show an approximately 80% decrease in the absorption maxima within 30 min. When the reaction time was increased to 90 min, PR-2–TiO_2 and PR-3–TiO_2 showed almost complete degradation of MB.

The degradation of MB dye follows pseudo-first-order kinetic and expressed with below equation [32–34].

$$\ln \left(C_0/C \right) = kt$$

In this equation, k is degradation rate constant in min^{-1}. The k values for bare TiO_2, PR-1–TiO_2, PR-2–TiO_2 and PR-3–TiO_2 are 0.32×10^{-2}, 1.11×10^{-2}, 4.71×10^{-2} and 5.22×10^{-2}, respectively. The higher k values for PR-2–TiO_2 and PR-3–TiO_2 evidence the superior catalytic degradation over bare TiO_2, PR-1–TiO_2 (Fig. 7c).

If we compare the degradation curve of the axial dihydroxy porphyrin photocatalyst with that of the general carboxylic-anchored porphyrin, in the first 30 min, PR-3–TiO_2 shows a slightly higher degradation rate in comparison with PR-2–TiO_2 and the same can be seen up to 60 min. The higher photodegradation activity of PR-3–TiO_2 is due to the carboxylic anchor making it easier to inject an electron [20]. For PR-2–TiO_2, the axially coordinated dihydroxy groups enable the porphyrin molecule to be perfectly parallel to the TiO_2 surface; hence, porphyrin molecules will easily accumulate on the TiO_2 surface, which facilitates electron transfer from the porphyrin to TiO_2. Additionally, tin complexes with axial coordination reduce the molecular interactions between porphyrin molecules, resulting in a lack of aggregation will increase efficiency [35].

The fluorescence lifetime (τ) results exhibited that compared to bare TiO_2 excited state lifetime, PR-2–TiO_2 and PR-3–TiO_2 showed almost double excited state lifetime. Therefore, the possibility of electron–hole recombination was decreased and leading to increase photocatalytic activity in porphyrin combined TiO_2 (Fig. 8). Finally, these results showed that tin-porphyrin complex showed almost similar photodegradation pattern in comparison with carboxylic acid porphyrin.

The PR-2–TiO_2 photocatalytic mechanism is shown in Scheme 2. First, tin-porphyrin–TiO_2 will absorb visible light to reach the excited state. After intersystem crossing, the excited molecule will react with molecular oxygen and triplet oxygen to produce radical oxygen and singlet oxygen [36, 37]. Simultaneously, at the hole position of TiO_2, water molecules will react and release $\cdot OH$ [38]. Finally, $\cdot O_2^-$, $^1O_2$, $\cdot OH$ and PR-1$^+$–TiO_2 will react with and degrade MB into CO_2 and H_2O (Scheme 2). The plausible diagram is shown in Fig. 8 to represent the interactions between the hydroxyl group of tin porphyrin and TiO_2 in the mechanistic approach (Fig. 9).
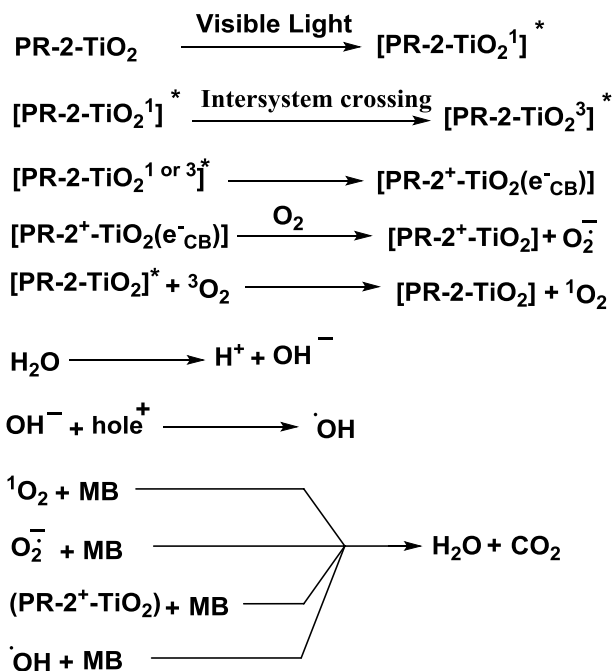
Stability studies

To evaluate and compare the long-term stability and reusability [39] of the prepared PR-2–TiO_2 and PR-3–TiO_2 nanoscale photocatalysts, we performed repeatability experiments. The experimental results show that our newly synthesized axial
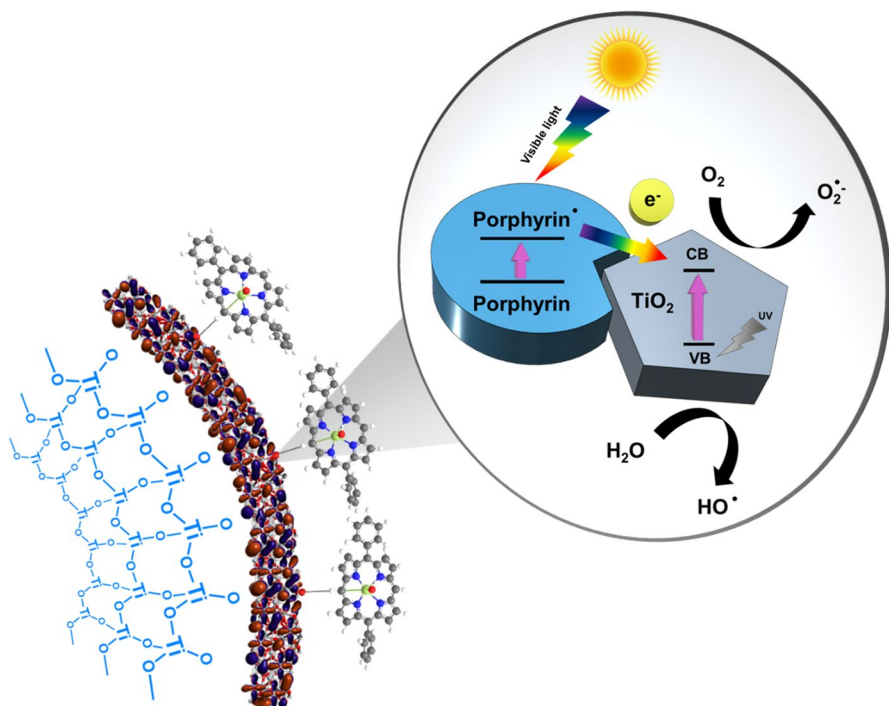
(a)

(b)

(c)
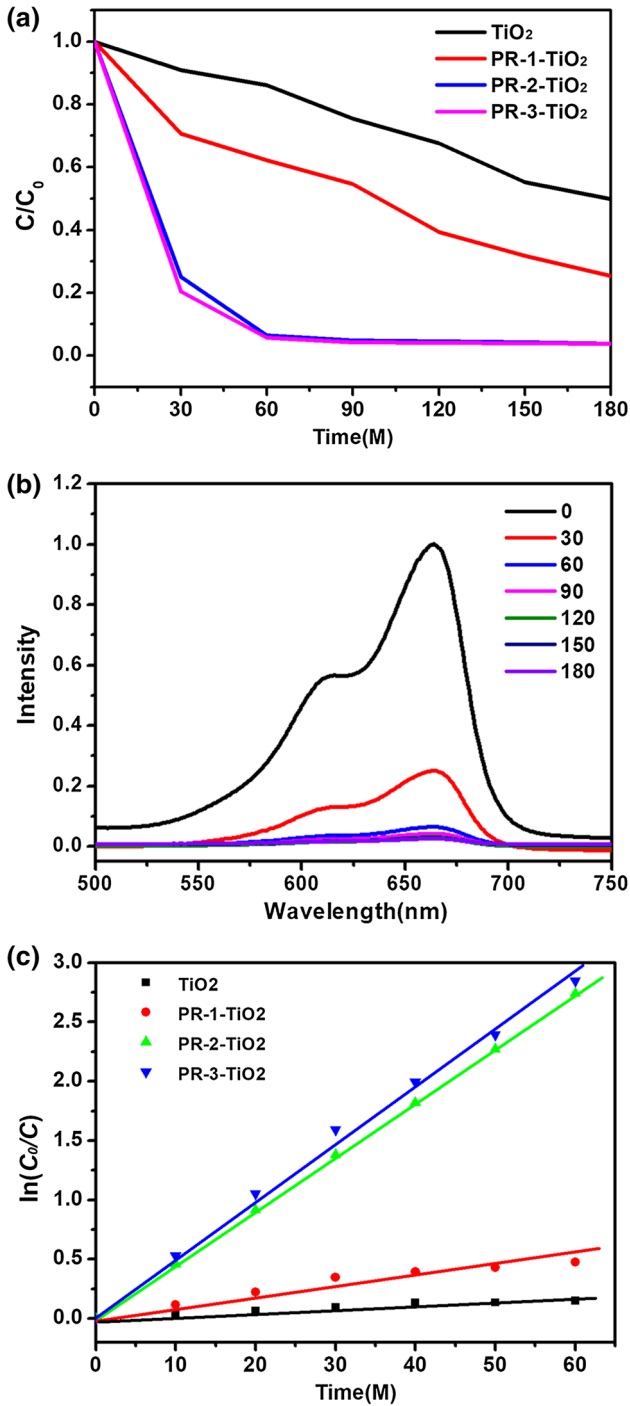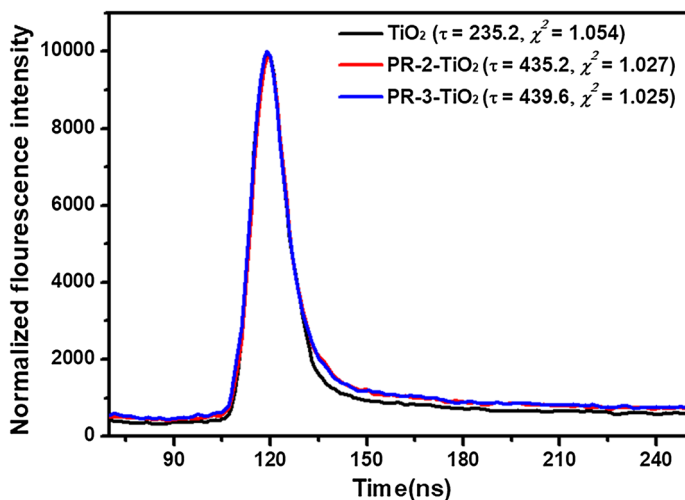
Fig. 8 Fluorescence decay profiles of bare TiO_2, PR-1–TiO_2, PR-2–TiO_2 and PR-3–TiO_2 using 340 nm LED as the excitation source

$$PR\text{-}2\text{-}TiO_2 \xrightarrow{\text{Visible Light}} [PR\text{-}2\text{-}TiO_2{}^1]^*$$

$$[PR\text{-}2\text{-}TiO_2{}^1]^* \xrightarrow{\text{Intersystem crossing}} [PR\text{-}2\text{-}TiO_2{}^3]^*$$

$$[PR\text{-}2\text{-}TiO_2{}^{1 \text{ or } 3}]^* \longrightarrow [PR\text{-}2^+\text{-}TiO_2(e^-{}_{CB})]$$

$$[PR\text{-}2^+\text{-}TiO_2(e^-{}_{CB})] \xrightarrow{O_2} [PR\text{-}2^+\text{-}TiO_2] + O_2^-$$

$$[PR\text{-}2\text{-}TiO_2]^* + {}^3O_2 \longrightarrow [PR\text{-}2\text{-}TiO_2] + {}^1O_2$$

$$H_2O \longrightarrow H^+ + OH^-$$

$$OH^- + hole^+ \longrightarrow {}^\cdot OH$$

$$\left.\begin{array}{l} {}^1O_2 + MB \\ O_2^- + MB \\ (PR\text{-}2^+\text{-}TiO_2) + MB \\ {}^\cdot OH + MB \end{array}\right\} \longrightarrow H_2O + CO_2$$

Scheme 2 Photocatalytic mechanism of PR-2–TiO_2

Fig. 9 Plausible diagram for the photocatalytic mechanism of PR-2–TiO$_2$

dihydroxyl tin photocatalyst (PR-2–TiO$_2$) exhibits comparable stability to the carboxylic-anchored porphyrin photocatalyst (PR-3–TiO$_2$). Both catalysts retain nearly 80% of their original photocatalytic efficiency after the fifth cycle. After the tenth cycle, both of the catalysts exhibit almost 60% of their original photocatalytic conversion efficiency (Fig. 10). These results suggest that PR-2–TiO$_2$ is stable under visible irradiation.

Theoretical studies

To gain insight into the electronic and optical properties, and optimized electron cloud density distributions of the dyes, theoretical investigations were carried out using the Gaussian 09 theoretical program [40] at the DFT/B3LYP level of theory, and the results are shown in Fig. 11. As shown in the figure, the simulated HOMO and LUMO energies are found to be -5.43 and -2.71 eV, -5.25 and -2.39 eV with band gaps of 2.72 and 2.86 eV for PR-2 and PR-3, respectively. Molecular orbital calculations on the two photocatalysts indicated that the HOMOs were mostly located on the pyrrole nitrogen and methane bridges. The LUMOs exhibit greater delocalization, being localized at the porphyrin core moiety. Upon excitation, the excited electron of the HOMO is transferred to the LUMO, and then the electron density of the π–π* is delocalized over the porphyrin, which induces efficient charge
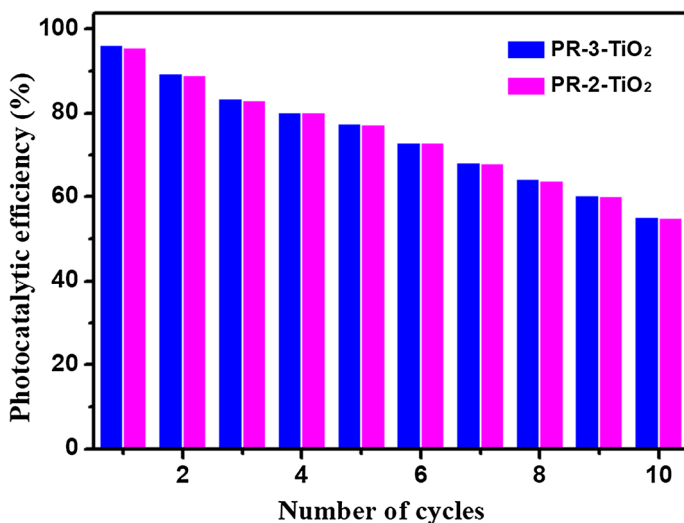
Fig. 10 Reusability studies of PR-2–TiO$_2$ and PR-3–TiO$_2$

transfer from the dye to the anatase TiO$_2$ surface. The energy of the valence band (VB) and conduction band (CB) and the band gap of anatase TiO$_2$ was taken from the previous report as shown in figure [41–43].

The HOMO, LUMO, band gap and electron density distribution pattern for both the dyes (**PR-2 and PR-3**) are similar, and the differences are small to negligible. From the above observations, it is found that the LUMO energy of the dyes is higher and matches the energy of the conduction band (CB) edge of TiO$_2$, and higher the intramolecular charge transfer within the porphyrin moiety, which are necessary for the valid and good carrier transfer.

Conclusion

Here, we designed and synthesized a new dihydroxotin(IV) porphyrin derivative and confirmed its structure by ^{1}H NMR, ^{13}C NMR, MALDI-TOF and FTIR spectral analysis. This PR-2 was grafted with TiO$_2$ to form the photocatalyst (PR-2–TiO$_2$). The PR-2–TiO$_2$, basic porphyrin (PR-1–TiO$_2$) and carboxylic-anchored porphyrin (PR-3–TiO$_2$) photocatalysts were confirmed by SEM, XRD, XPS and diffuse reflectance spectra. After comparing the PR-2–TiO$_2$ photocatalytic results with those of PR-1–TiO$_2$ and PR-3–TiO$_2$ for the degradation of MB under visible light conditions, we concluded that PR-1–TiO$_2$ showed the least MB degradation activity, which was better than that of bare TiO$_2$. However, the carboxylic-anchored porphyrin (PR-3–TiO$_2$) and dihydroxyl tin complexes (PR-2–TiO$_2$) exhibited similar MB degradation to one another. Furthermore, we explained the mechanism of the PR-2–TiO$_2$ photocatalytic process. Recycling experiments have shown that the PR-2–TiO$_2$ photocatalyst is stable and can be reused. In our experiments, we
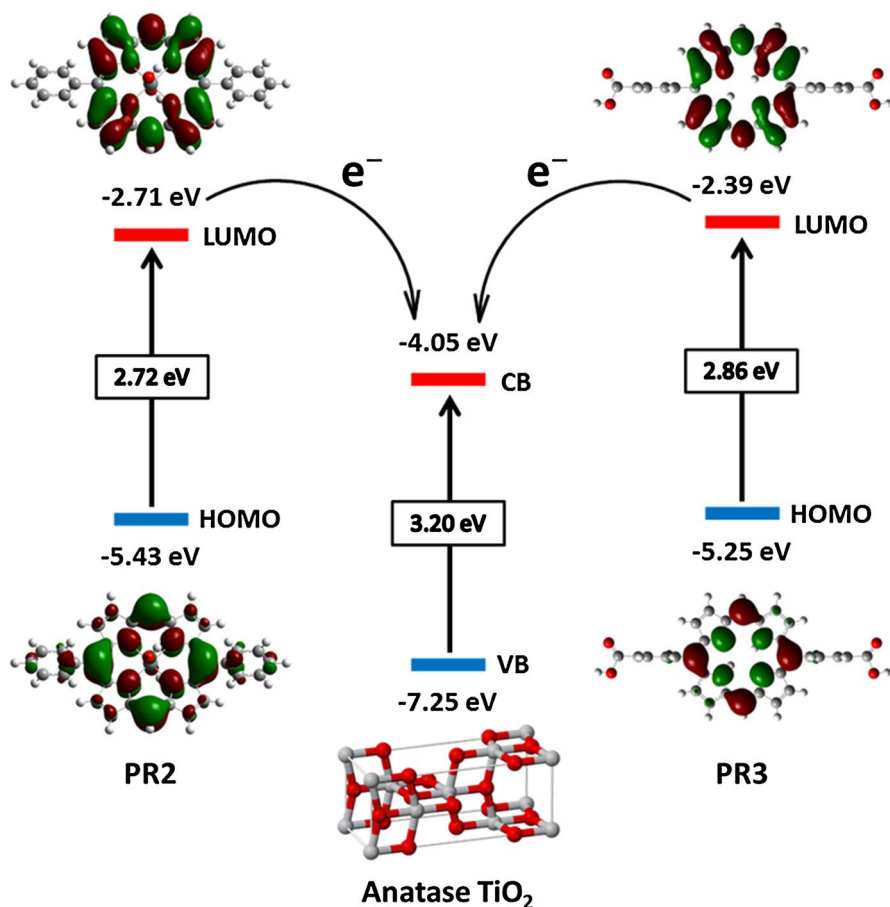
Fig. 11 Energy level diagram of PR-2, PR-3 and anatase TiO_2, and electronic cloud density distribution of two dyes (PR-2 and PR-3)

concluded that such axially coordinated dihydroxy tin porphyrin complexes will play a key role in the area of photocatalysis and also the tin-porphyrin photocatalysts are the alternative option for carboxylic anchor porphyrin photocatalysts.

References

1. T.L. Thompson, J.T. Yates Jr., Chem. Rev. **106**, 4428 (2006)
2. X.B. Chen, S.S. Mao, Chem. Rev. **107**, 2891 (2007)
3. X.B. Chen, C. Burda, J. Am. Chem. Soc. **130**, 5018 (2008)
4. J. Ananpattarachai, P. Kajitvichyanukul, S. Seraphin, J. Hazard. Mater. **168**, 253 (2009)

5. G. Mele, R.D. Sole, G. Vasapollo, E.G. López, L. Palmisano, M. Schiavello, J. Catal. **217**, 334 (2003)
6. J. Wang, J. Li, Y.P. Xie, C.W. Li, G.X. Han, L.Q. Zhang, R. Xu, X.D. Zhang, J. Environ. Manag. **91**, 677 (2010)
7. S. Chu, X. Zheng, F. Kong, G. Wu, L. Luo, Y. Guo, H. Liu, Y. Wang, H. Yu, Z. Zou, Mater. Chem. Phys. **129**, 1184 (2011)
8. A. Hagfeld, G. Boschlo, L. Sun, L. Kloo, H. Pettersson, Chem. Rev. **110**, 6595 (2010)
9. H.Y. Huang, X.T. Gu, J.H. Zhou, K. Ji, H.L. Liu, Y.Y. Feng, Catal. Commun. **11**, 58 (2009)
10. P. Moro, M.P. Donzello, C. Ercolani, F. Monacelli, G. Moretti, J. Photochem. Photobiol. A **220**, 77 (2011)
11. Y. Chen, A. Li, Z.H. Huang, L.N. Wang, F. Kang, Nanomaterials **6**, 51 (2016)
12. K. Morita, K. Takijiri, K. Sakai, H. Ozawa, Dalton Trans. **46**, 15181 (2017)
13. D.G. Whitten, J.C.N. Yau, F.A. Carroll, J. Am. Chem. Soc. **93**, 2291 (1971)
14. D.P. Arnold, J. Blok, Coord. Chem. Rev. **248**, 299 (2004)
15. H.J. Kim, N.K. Shee, K.-M. Park, H.-J. Kim, Inorg. Chim. Acta **488**, 1 (2019)
16. W. Kim, J. Park, H.J. Jo, H.-J. Kim, W. Choi, J. Phys. Chem. C **112**, 491 (2008)
17. S. Wang, I. Tabata, K. Hisada, T. Hori, J. Porphyr. Phthalocyanines **7**, 199 (2003)
18. G.D. Fallon, M.A.-P. Lee, S.J. Langford, P.J. Nichols, Org. Lett. **4**, 1895 (2002)
19. M.Y. Duan, J. Li, G. Mele, C. Wang, X.F. Lu, V. Giuseppe, F.X. Zhang, J. Phys. Chem. C **114**, 7857 (2010)
20. K.S. Min, R.S. Kumar, J.H. Lee, K.S. Kim, S.G. Lee, Y.-A. Son, Dyes Pigments **160**, 37 (2019)
21. K.S. Min, R. Manivannan, Y.-A. Son, Dyes Pigments **162**, 8 (2019)
22. H. Kim, R. Manivannan, G. Heo, J.W. Ryu, Y.-A. Son, Res. Chem. Intermed. **45**, 1 (2019)
23. R.S. Kumar, H. Jeong, J. Jeong, R.K. Chitumalla, M.J. Ko, K.S. Kumar, J. Jange, Y.-A. Son, RSC Adv. **6**, 41294 (2016)
24. J. Jeong, R.S. Kumar, N. Mergu, Y.-A. Son, Inorg. Chim. Acta **469**, 453 (2018)
25. M.A. Ahmed, Z.M. Abou-Gamra, H.A.A. Medien, M.A. Hamza, J. Photochem. Photobiol. B **176**, 25 (2017)
26. W. Li, R. Liang, A. Hu, Z. Huang, Y.N. Zhou, RSC Adv. **4**, 36959 (2014)
27. C. Huang, Y. Lv, Q. Zhou, S. Kanga, Q. Xl, J. Mu, Ceram. Int. **40**, 7093 (2014)
28. G.M. Bancroft, I. Adams, H. Lampe, T.K. Sham, J. Electron Spectrosc. Relat. Phenom. **9**, 191 (1976)
29. G.T. Baronetti, S.R. de Miguel, O.A. Scelza, A.A. Castro, Appl. Catal. **24**, 109 (1986)
30. G. Mele, R.D. Sole, G. Vasapollo, G. Marcı, V. GarcıaLopez, L. Palmisano, J.M. Coronado, M.D.H. Alonso, C. Malitesta, M.R. Gualcito, J. Phys. Chem. B **109**, 12347 (2005)
31. J. Yu, G. Dai, Q. Xiang, M. Jaroniec, J. Mater. Chem. **21**, 1049 (2011)
32. F. Chen, Y. Cao, D. Jia, Chem. Eng. J. **234**, 223 (2013)
33. H. Pouretedal, M. Keshavarz, Int. J. Phys. Sci. **6**, 6268 (2011)
34. Z.-X. Li, B.-L. Yang, Y.-F. Jiang, C.-Y. Yu, L. Zhang, Cryst. Growth Des. **18**, 979 (2018)
35. H.J. Jo, S.H. Jung, H.-J. Kim, Bull. Korean Chem. Soc. **25**, 1869 (2004)
36. C.J.P. Monteiro, M.M. Pereira, M.E. Azenha, H.D. Burrows, C. Serpa, L.G. Arnaut, M.J. Tapia, M. Sarakha, P. Wong-Wah-Chung, S. Navaratnam, Photochem. Photobiol. Sci. **4**, 617 (2005)
37. F.L. Guern, C.F. Bied-Charreton, J. Bull. Soc. Chim. Fr. **130**, 753 (1993)
38. V. Etacheri, C.D. Valentin, J. Schneider, D. Bahnemann, S.C. Pillai, J. Photochem. Photobiol. C Photochem. Rev. **25**, 1 (2015)
39. X. Zhao, Y. Wang, W. Feng, H. Lei, J. Li, RSC Adv. **7**, 52738 (2017)
40. M.J. Frisch, G.W. Trucks, H.B. Schlegel, G.E. Scuseria, M.A. Robb, J.R. Cheeseman, G. Scalmani, V. Barone, B. Mennucci, G.A. Petersson et al., *Gaussian 09, Revision B.01* (Gaussian Inc., Wallingford, 2010)
41. J. Fujisawa, T. Eda, M. Hanaya, Chem. Phys. Lett. **685**, 23 (2017)
42. J. Jeong, R.S. Kumar, N. Mergu, Y.-A. Son, J. Mol. Struct. **1147**, 469 (2017)
43. C. Kim, R.S. Kumar, N. Mergu, K. Jun, Y.A. Son, J. Nanosci. Nanotechnol. **18**, 3192 (2017)

Publisher's Note Springer Nature remains neutral with regard to jurisdictional claims in published maps and institutional affiliations.